

## On the Connection between the Mediterranean Outflow and the Azores Current

TAMAY M. ÖZGÖKMEN, ERIC P. CHASSIGNET, AND CLAES G. H. ROTH

*RSMAS/MPO, University of Miami, Miami, Florida*

(Manuscript received 18 August 1999, in final form 19 April 2000)

### ABSTRACT

As the salty and dense Mediterranean overflow exits the Strait of Gibraltar and descends rapidly in the Gulf of Cadiz, it entrains the fresher overlying subtropical Atlantic Water. A minimal model is put forth in this study to show that the entrainment process associated with the Mediterranean outflow in the Gulf of Cadiz can impact the upper-ocean circulation in the subtropical North Atlantic Ocean and can be a fundamental factor in the establishment of the Azores Current. Two key simplifications are applied in the interest of producing an economical model that captures the dominant effects. The first is to recognize that in a vertically asymmetric two-layer system, a relatively shallow upper layer can be dynamically approximated as a single-layer reduced-gravity controlled barotropic system, and the second is to apply quasigeostrophic dynamics such that the volume flux divergence effect associated with the entrainment is represented as a source of potential vorticity.

Two sets of computations are presented within the  $1\frac{1}{2}$ -layer framework. A primitive-equation-based computation, which includes the divergent flow effects, is first compared with the equivalent quasigeostrophic formulation. The upper-ocean cyclonic eddy generated by the loss of mass over a localized area elongates westward under the influence of the  $\beta$  effect until the flow encounters the western boundary. In the steady state, the circulation pattern consists of bidirectional zonal flows with a limited meridional extent: eastward to the south of the sink and westward to the north of the sink. The localized sink drives a horizontal circulation in the interior ocean whose strength is approximately an order of magnitude greater than the sink's strength. It is demonstrated that the induced circulation in the far field from a localized sink is insensitive to the neglect of the divergent flow component.

A set of parameter sensitivity experiments is then undertaken with the quasigeostrophic model for an idealized midlatitude circulation, driven both by wind forcing and "thermohaline" flow through the open southern and northern boundaries. When a sink near the eastern boundary is superimposed on the idealized midlatitude circulation, it is shown to alter significantly the upper-ocean flow and induce an eastward zonal current, which resembles the Azores Current in location and transport. This mechanism also generates a westward current to the north of the sink location, which could be associated with the Azores Countercurrent. An extensive series of sensitivity experiments is conducted to determine the response of this current system to changes in the boundary layer processes, sink strength, sink distribution, model resolution, and wind forcing. The magnitude of the current transports is found to be sensitive to the sink intensity and to its distance from the coastline.

### 1. Introduction

Despite that the North Atlantic Ocean is the most observed and investigated of all the world's oceans, many features of its circulation are still not accurately understood. Compared to flows along the western boundary, the currents in the eastern Atlantic are relatively weak, and little information exists with regard to their structures. It is not entirely clear where and how the return flow in the eastern North Atlantic takes place. For instance, in his widely reproduced basic current diagram for the North Atlantic Ocean, Worthington (1976) concentrates nearly the entire circulation on the

western side of the Mid-Atlantic Ridge. On the other hand, Dietrich et al. (1975) show a northward turn of the Gulf Stream at the Flemish Cap as the North Atlantic Current and another branch flowing to the east and crossing the Mid-Atlantic Ridge. More recent depictions of the North Atlantic circulation by Schmitz and McCartney (1993) incorporate both perspectives.

The existence of a well-defined circulation branch extending almost purely zonally between southeast of the Grand Banks and the Gulf of Cadiz has been identified relatively recently and referred to as the Azores Current (hereafter referred to as AzC) (Gould 1985; Stramma 1984; Klein and Siedler 1989). The AzC is surmised to provide a significant portion of the upper-ocean transport to the basin east of the Mid-Atlantic Ridge (Käse and Siedler 1982; Gould 1985; Käse et al. 1985). Figure 1a depicts the horizontal velocity field at 500-m depth derived by Olbers et al. (1985) from a  $\beta$ -spiral analysis of the Levitus (1982) dataset. The split-

---

*Corresponding author address:* Tamay Ozgokmen, RSMAS/MPO, University of Miami, 4600 Rickenbacker Causeway, Miami, FL 33149-1098.  
E-mail: tozgokmen@rsmas.miami.edu

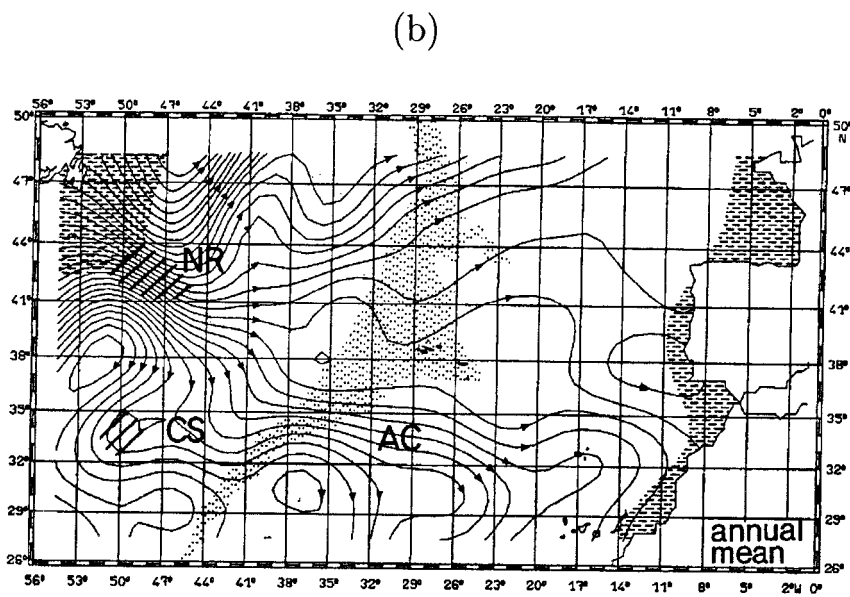
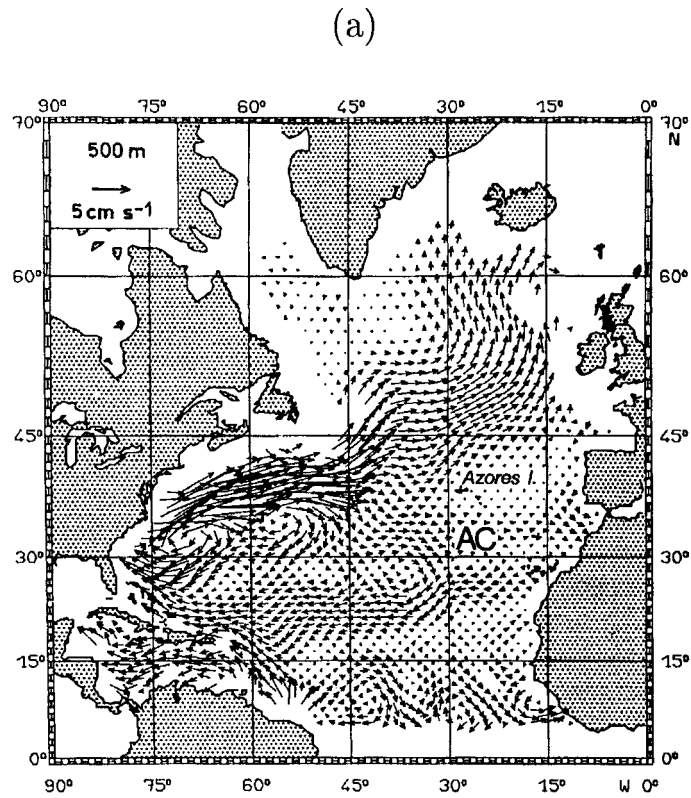


FIG. 1. (a) Horizontal velocities at 500-m depth obtained from a beta-spiral analysis by Olbers et al. (1985). The Azores Current is indicated by AC. (b) Annual mean volume transport streamlines in the layer 0–800 m calculated by Klein and Siedler (1989) (contour interval CI = 1.5 Sv).

ting of the Gulf Stream into a recirculating flow, the North Atlantic Current, and the AzC is apparent south of the Grand Banks. Klein and Siedler (1989) calculated annual mean geostrophic flow fields from hydrographic data (Fig. 1b). The zonal extent of the AzC stretches from the transition zone between the Gulf Stream and the North Atlantic Current in the area of the southeastern Newfoundland Rise all the way to the eastern boundary. Meridionally, the AzC is located at latitudes from approximately  $32^{\circ}$  to  $35^{\circ}$ N. The eastward transport of the AzC is estimated from historic hydrographic data and CTD measurements to be 8–12 Sv ( $\text{Sv} \equiv 10^6 \text{ m}^3 \text{ s}^{-1}$ ), with most of the transport concentrated in the upper 1000 m of the ocean and with velocities exceeding  $0.1 \text{ m s}^{-1}$  (Gould 1985; Stramma 1984; Stramma and Müller 1989).

The reasons for the existence of the AzC have not been clearly established (Spall 1990). Wind and buoyancy forcing mechanisms have been put forward [see Käse and Krauss (1996) for a review], but do not explain why the position of the observed AzC does not change despite large seasonal latitudinal variations (on the order of 1000 km) in wind and buoyancy forcing. Satellite observations (Le Traon and De Mey 1994) show that the axis of the AzC is located on average at the latitude of the Strait of Gibraltar and that there is very little seasonal variation in its position. Compelling circumstantial evidence has been produced by recent numerical studies that show there is a direct link between the emergence of an AzC in a realistic OGCM, the Miami Isopycnic Coordinate Ocean Model (MICOM), and inclusion of water mass transformation processes in the Gulf of Cadiz (Jia 2000). The latter were induced by the relaxation of the water density fields toward climatological conditions, as a means of representing the effect of exchange flows between the Mediterranean Sea and the Atlantic Ocean. When these processes are excluded from the model, the flow pattern identified with the AzC fails to appear, leading Jia (2000) to suggest that they play an essential role in the observed circulation. As illustrated in Fig. 2, subtropical gyre simulations by Paiva et al. (2000) and Chassignet et al. (2000, manuscript submitted to *J. Geophys. Res.*) with the same model also support this interpretation, despite the different resolution ( $1/2^{\circ}$ ) and domain configuration.

In the Mediterranean Sea, an average net evaporation rate of  $60 \text{ cm yr}^{-1}$  produces water that has approximately 2.1 ppt higher salinity than the exterior North Atlantic Water (NAW) (Kinder and Bryden 1987). The exchange between the Atlantic Ocean and the Mediterranean Sea takes place through the Strait of Gibraltar and, to first order, can be described as a two-layer flow (Bryden and Kinder 1991). The NAW flows into the Mediterranean in the upper layer at a rate of about 0.95 Sv, and the Mediterranean Water (MW) flows out of the Mediterranean in the lower layer at a rate of about 0.79 Sv (Bryden et al. 1989). The MW then descends the continental shelf in the Gulf of Cadiz (commonly known

as the Mediterranean Undercurrent at this stage) and mixes with the overlying NAW. Consequently, the transport of the MW increases by 100%–200% over a short distance by entraining NAW. Most recent estimates indicate that the MW entrains approximately 1.2 Sv of NAW (Baringer and Price 1997a), with most of the entrainment taking place over a distance of approximately 40–50 km and with entrainment rates on the order of  $10^{-3} \text{ m s}^{-1}$  in areas of large increase in transport (Baringer and Price 1997b; their Fig. 7a). The interaction of the Mediterranean Sea with the Atlantic Ocean near the Strait of Gibraltar is schematically depicted in Fig. 3. Since this transformation process takes place near the eastern boundary of the ocean basin, it has the potential to influence the entire basin circulation by the propagation of potential vorticity anomalies along the characteristics of the flow induced by the  $\beta$  effect and the wind field.

In the present study, we investigate the impact of this particular entrainment process on the upper-ocean circulation. The questions that we address are: (i) What kind of circulation patterns does a localized sink of fluid near the eastern boundary of an ocean basin generate? (ii) Can a localized sink of the observed magnitude [i.e.,  $O(1 \text{ Sv})$ ] drive basin-scale circulation patterns that are strong enough to interfere with and modify the wind-driven circulation? (iii) In particular, can a localized sink near the eastern boundary of an ocean basin exert a controlling influence on the location and transport of zonal current systems, such as the AzC?

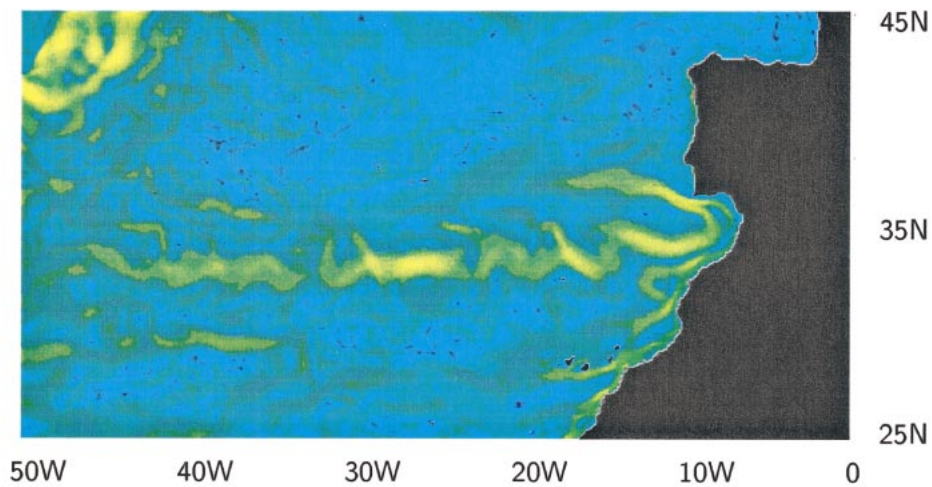
We address these questions by using a  $1\frac{1}{2}$ -layer quasigeostrophic (QG) model in idealized configurations. The fluid sink in the active layer is represented as a potential vorticity source [justified both by analytical arguments and by a comparison with results obtained with a primitive-equation model (MICOM)]. An extensive process study is conducted to determine the sensitivity of the induced circulation to factors such as the strength of the sink, sink distribution, interaction with the eastern boundary, model resolution, and wind forcing.

The paper is organized as follows. The basic theory behind flows created by a localized sink is briefly reviewed in section 2. In section 3, the impact of divergent and nonlinear effects on the large-scale induced circulation is analyzed numerically. The interaction of such flows with the wind-driven circulation is then investigated in section 4 and discussed in section 5. Summary and conclusions follow in section 6.

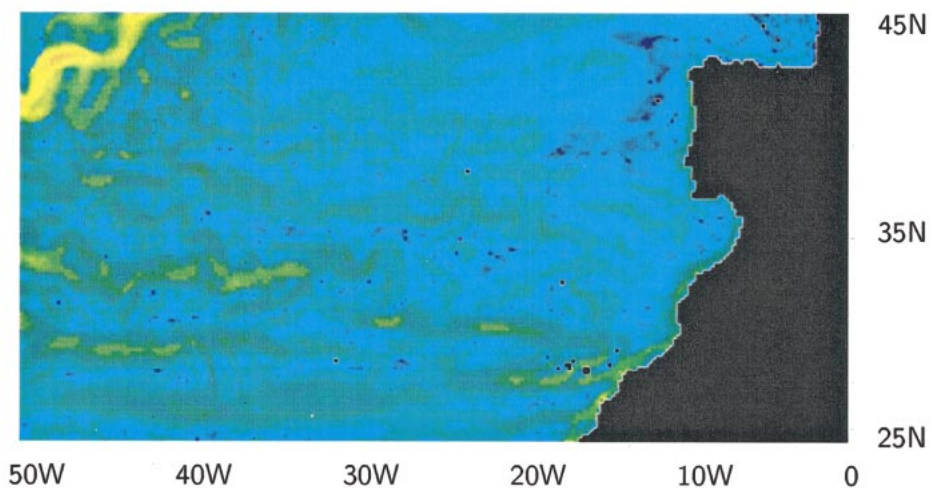
## 2. Theoretical arguments

The study of the circulation driven by sources and sinks of mass has a long history in oceanography, primarily because of the sinking induced by strong cooling near the polar regions and its impact on the thermohaline circulation. Stommel et al. (1958) analyzed the flow patterns generated by localized sources and sinks in a

## (a) With Mediterranean



## (b) Without Mediterranean



$\log_{10}$  energy ( $m^2/s^2$ ), min: -8 ; max: 1



FIG. 2. Surface-layer mean kinetic energy in high-resolution ( $1/2^\circ$ ) MICOM North Atlantic basin simulations (Chassignet et al.) (a) with a relaxation zone in the Gulf of Cadiz for the Mediterranean outflow and (b) without the relaxation. Note the existence of a prominent model AzC in (a).

homogeneous fluid on a  $\beta$  plane. The dynamical ideas developed on the basis of these experiments were then extended to develop a theory for the abyssal oceanic circulation (Stommel and Arons 1960a,b). It is a central feature of the theory by Stommel and Arons (1960a,b) that fluid motion between sources and sinks in a rotating

system may be accompanied by recirculating flows that have higher transports than those due to mass conservation (e.g., from a source to a sink). Understanding of this behavior is achieved by arguments based on potential vorticity conservation. The dynamics involved here are essentially the same as the “beta plume” ar-

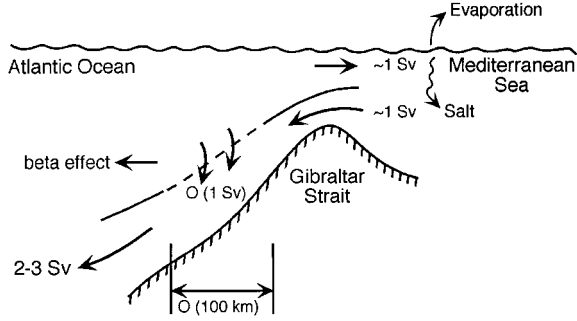


FIG. 3. Schematic illustration of the interaction of the eastern North Atlantic Ocean with the Mediterranean outflow in the Gulf of Cadiz. Note that the entrainment of the North Atlantic Water into the Mediterranean outflow takes place over a short distance. The resulting potential vorticity anomaly is subject to propagation along the entire basin.

guments invoked by Stommel (1982) as an explanation for the westward extended chemical signature distribution originating along the East Pacific Rise, and as those derived by Pedlosky (1996) for isolated sources/sinks.

The linearized reduced gravity equations in a Cartesian coordinate system assuming hydrostatic, steady, and frictionless motions can be written as

$$-fv = -g' \frac{\partial \eta}{\partial x}, \quad (1)$$

$$fu = -g' \frac{\partial \eta}{\partial y}, \quad (2)$$

$$\frac{\partial u}{\partial x} + \frac{\partial v}{\partial y} = -\frac{w_s}{H}, \quad (3)$$

where  $\eta$  is the interface displacement,  $f = f_0 + \beta y$ , and  $w_s(x, y) > 0$  represents loss of fluid from the active layer. Taking the curl of (1) and (2), we get the familiar Sverdrup relation,

$$v = \frac{f}{\beta H} w_s, \quad (4)$$

which states that for  $w_s > 0$ ,  $v > 0$ , implying northward flow, except in the western boundary layer where (4) fails. From (1) and (2), using the boundary condition  $\eta = 0$  at the eastern boundary  $x = x_e$ , the zonal velocity component becomes

$$u = \frac{1}{f\beta H} \int_x^{x_e} \frac{\partial}{\partial y} [f^2 w_s(x', y)] dx'. \quad (5)$$

It can be seen from (5) that for a source distribution that increases with latitude until it reaches an extremum and then decreases again, the zonal velocity is eastward south of the extremum and westward north of the extremum. The zonal flow is therefore bidirectional [see Fig. 7.4.1 of Pedlosky (1996)].

Rewriting (5),

$$uH = \int_x^{x_e} \left[ w_s(x', y) + \frac{1}{\beta} \frac{\partial}{\partial y} (f w_s(x', y)) \right] dx'. \quad (6)$$

The first term on the right-hand side of (6) represents the component of the zonal flow induced by mass imbalance and is eastward for  $w_s > 0$  (towards the sink). The second term is the bidirectional or recirculating component. The ratio of the first term to the second term is equal to  $L_w/(R \tan \lambda)$  where  $L_w$  is the meridional size of the source distribution,  $R$  the radius of the earth, and  $\lambda$  the latitude. Hence, for localized sinking at mid-latitudes, the mass imbalance-driven component is negligible with respect to the recirculating component. Equation (6) also indicates that the zonal flows are restricted to the meridional extent of the sinking zone.

The resulting zonal transport is then

$$\int_{y_1}^{y_2} uH dy = \int_{y_1}^{y_2} \int_x^{x_e} w_s dx dy + \frac{1}{\beta} \int_x^{x_e} f w_s \Big|_{y=y_1}^{y=y_2} dx, \quad (7)$$

where  $y_1$  and  $y_2$  indicate the latitudes chosen for integration. Again, the first term on the right-hand side of (7) is equal to the mass flow rate entrained from the active layer into the abyss, over the extent of the circulation. The second term is the recirculating component, which integrates to zero with no net zonal flux, over a distance equal to or larger than the meridional extent of the circulation.

In summary: (i) Nonzero velocities exist only near the sinking region or directly west of it. (ii) The zonal flow consists of two components: the mass imbalance-driven and recirculating flow. For localized sinks, the recirculating component is much larger than the mass flux component. (iii) The recirculating zonal component is eastward to the south of the sink center (for  $w_s > 0$ ) and westward to the north of the sink center. Therefore, the circulation is cyclonic for a loss of mass. (iv) The meridional extent of the circulation is limited to that of the sink, but frictional effects, not considered in the above analysis, may play a role in controlling it. This issue will become clearer in the following discussion of the numerical experiments.

### 3. Large-scale circulation patterns induced by a localized sink

#### a. Model configuration

The simplest model that allows an interior fluid sink is equivalent barotropic ( $1\frac{1}{2}$  layer). One can justify this choice by considering that the entrainment process associated with the Mediterranean outflow takes place in the upper ocean (i.e., at a depth of 500–1000 m; Arhan 1987), which makes the velocities in the deeper ocean much smaller than those in the upper ocean. Quasigeostrophic dynamics will be used by representing the sink as a potential vorticity source. The neglect of the divergent flow (i.e., flows driven by the mass imbalance)

TABLE 1. Common parameters of the numerical simulations A1–A3. The sink is located at  $x = 5700$  km and  $y = 1000$  km (considering the southwest corner as the origin).

Basin size ( $x, y$ )	6000 km $\times$ 2000 km
Coriolis parameters	$f_0 = 7.3 \times 10^{-5} \text{ s}^{-1}$ $\beta = 2 \times 10^{-11} \text{ m}^{-1} \text{ s}^{-1}$
Layer thickness	$H = 1000$ m
Reduced gravity	$g' = 0.01 \text{ m s}^{-2}$
Deformation radius	$R_d = 42$ km
Eddy viscosity	see Table 1
Horizontal grid scale	see Table 1
Entrainment volume flux	1 Sv
Entrainment velocity scale	$6 \times 10^{-4} \text{ m s}^{-1}$

is justified in section 3b by comparing the model results to those obtained from a primitive equation model (MICOM) with an actual fluid sink.

The quasigeostrophic reduced gravity model equations are

$$\frac{\partial q}{\partial t} + J(\psi, q) = \frac{f_0}{H}(w_E + w_S) + \nu \nabla^4 \psi, \quad (8)$$

where  $q$  is the potential vorticity defined by

$$q = \nabla^2 \psi + \beta y - \frac{1}{R_d^2} \psi. \quad (9)$$

Here  $\psi$  is the geostrophic streamfunction,  $f_0$  the Coriolis frequency at a reference latitude,  $\beta$  the meridional gradient of the Coriolis frequency,  $R_d = \sqrt{g'H}/f_0$  the radius of deformation,  $g'$  the reduced gravity,  $H$  the active layer depth,  $w_E$  the Ekman velocity field proportional to the wind stress curl,  $w_S$  the entrainment velocity field associated with the sink,  $\nu$  the horizontal eddy viscosity, and  $\nabla^2 = \partial^2/\partial x^2 + \partial^2/\partial y^2$  the Laplacian. A nondimensionalized form of the prognostic equation (8) is advanced in time using a predictor-corrector type of leapfrog method (Gazdag 1976). The Jacobian operator

$$J(\psi, q) = \frac{\partial \psi}{\partial x} \frac{\partial q}{\partial y} - \frac{\partial q}{\partial x} \frac{\partial \psi}{\partial y}$$

is computed using the formulation proposed by Arakawa (1966) that conserves kinetic energy and enstrophy, and satisfies the antisymmetry property  $J(\psi, q) = -J(q, \psi)$ . The diagnostic equation (9) is inverted using a relaxation method.

The model is initially configured in a domain with a zonal dimension of 6000 km, and a meridional extent of 2000 km, centered at 30°N. The equilibrium layer thickness is taken as 1000 m, and the stratification is such that the Rossby radius of deformation is approx-

imately 42 km, typical of midlatitude circulation. The system is driven purely by a sink represented as a potential vorticity source, located 300 km from the eastern boundary at  $x = 5700$  km in the middle of the basin ( $y = 1000$  km), and active over a single grid point. The sink is far enough from the eastern boundary such that their interaction is negligible. The entrainment velocity scale  $w_S$  is set equal to  $6 \times 10^{-4} \text{ m s}^{-1}$  and corresponds to 1 Sv of fluid transfer (Baringer and Price 1997a,b) from the active upper layer into the motionless abyss.

In order to estimate the importance of the divergent flow contribution, a 1½-layer version of MICOM (Bleck and Chassignet 1994) is identically configured with a sink prescribed in the continuity equation, and compensated for by small fluid injection at all grid points along the southern and northern boundaries so that the total volume in the active layer is conserved at all times. The parameters of the experiments are summarized in Tables 1 and 2.

### b. Numerical simulations

We first compare the MICOM experiment (experiment A1) to the QG experiment (experiment A2) in order to verify that the representation of volume flux divergence as potential vorticity flux is a reasonably good approximation, therefore justifying the use of a quasigeostrophic model in the remainder of this study. These first two experiments are conducted using a low resolution (Table 2) and reach a steady state (no eddy activity). The importance of resolving the Rossby radius of deformation will be addressed in experiment A3. The results of experiment A1 are shown in Fig. 4. The upper layer stretches by the downward velocity associated with loss of fluid and a cyclonic circulation is induced via conservation of potential vorticity. Initially, the cyclonic circulation has the shape of an axisymmetric eddy, which then begins to propagate westward due to the  $\beta$  effect. Since the source of the eddy is fixed in space, this propagation takes place as an elongation of the vortex (Fig. 4a). In experiment A1, the westward elongation of the cyclonic vortex persists until the flow encounters the western boundary, where friction becomes important. Frictional effects are also important near the sink and control the meridional extent of the circulation. Figure 4b depicts the interface displacement and Fig. 4c shows the velocity field in the steady state. Signs of divergence are evident near the location of the sink. Consistent with the theoretical description given in section 2, the steady-state circulation pattern consists

TABLE 2. List of numerical experiments described in section 3b.

Expt	Model	Resolution (km)	Viscosity, $\nu$ ( $\text{m}^2 \text{ s}^{-1}$ )	Forcing
A1	MICOM	40	1000	Volume flux
A2	QG	40	1000	PV flux
A3	QG	10	50	PV flux

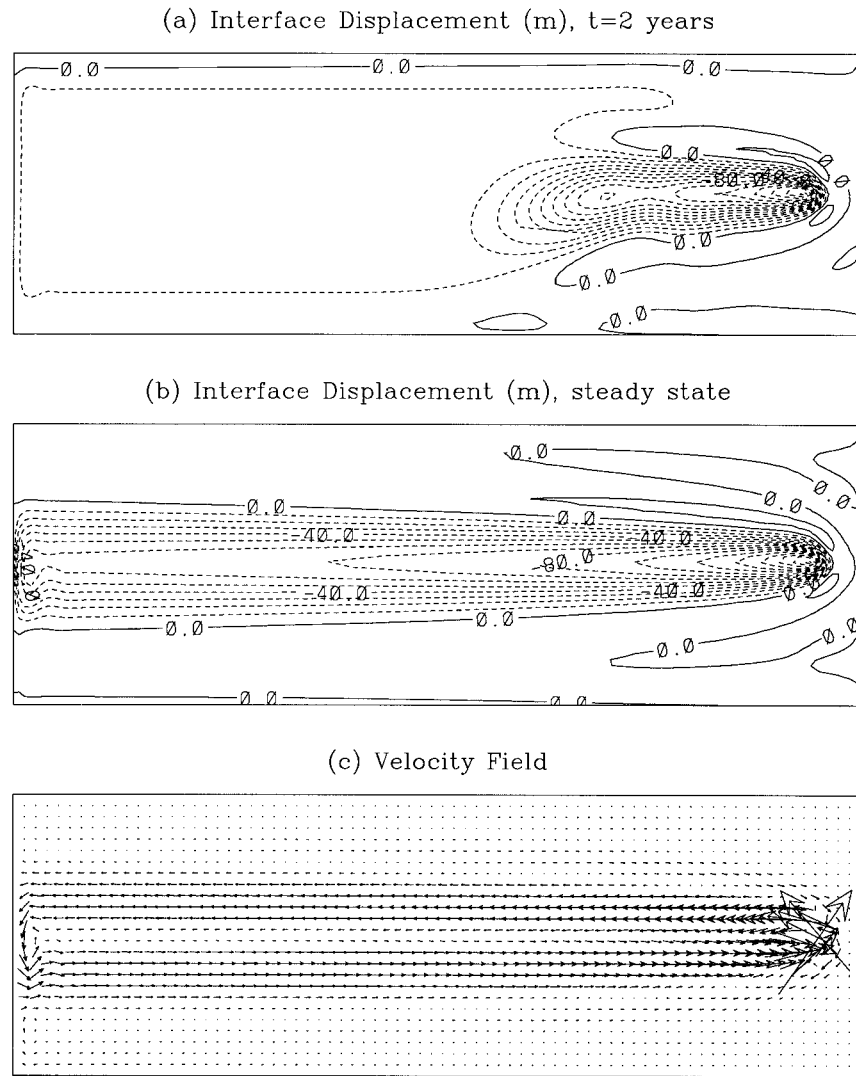


FIG. 4. (a) Interface displacement at  $t = 2$  yr ( $CI = 10$  m), (b) steady-state interface displacement ( $CI = 10$  m), and (c) steady-state velocity field (maximum vector:  $25 \text{ cm s}^{-1}$ ) for reduced-gravity MICOM simulation (expt A1).

of bidirectional zonal flows with a limited meridional extent: eastward to the south of the sink and westward to the north of the sink.

Results of the quasigeostrophic run with equivalent parameters (experiment A2) to those of the primitive equation experiment are shown in Fig. 5. The primary conceptual difference from experiment A1 is that in experiment A2 the flow is nondivergent, hence flows driven by mass imbalance are not represented, whereas experiment A1 includes this effect. A comparison of Figs. 4b and 5b demonstrates that the difference between the interface displacements is hardly distinguishable. The velocity fields (Figs. 4c and 5c) are also essentially the same, except in close proximity of the sink location, where the effect of divergence is important. Figure 5a

depicts the steady-state transport streamfunction (not appropriate to plot in A1 since the flow is divergent).

The essential point in these two simulations is that a potential vorticity sink that corresponds to a volume sink of  $1 \text{ Sv}$  generates a circulation of approximately  $8\text{--}10 \text{ Sv}$  over the entire zonal extent of the domain. The main circulation pattern is induced by the conservation of potential vorticity rather than by the conservation of mass, and the localized sink drives a horizontal circulation whose strength is an order of magnitude greater than its own strength. The agreement of experiments A1 and A2 justifies the use of the quasigeostrophic model for the present study.

The bidirectional jet pattern present in the experiments is likely to become barotropically unstable be-

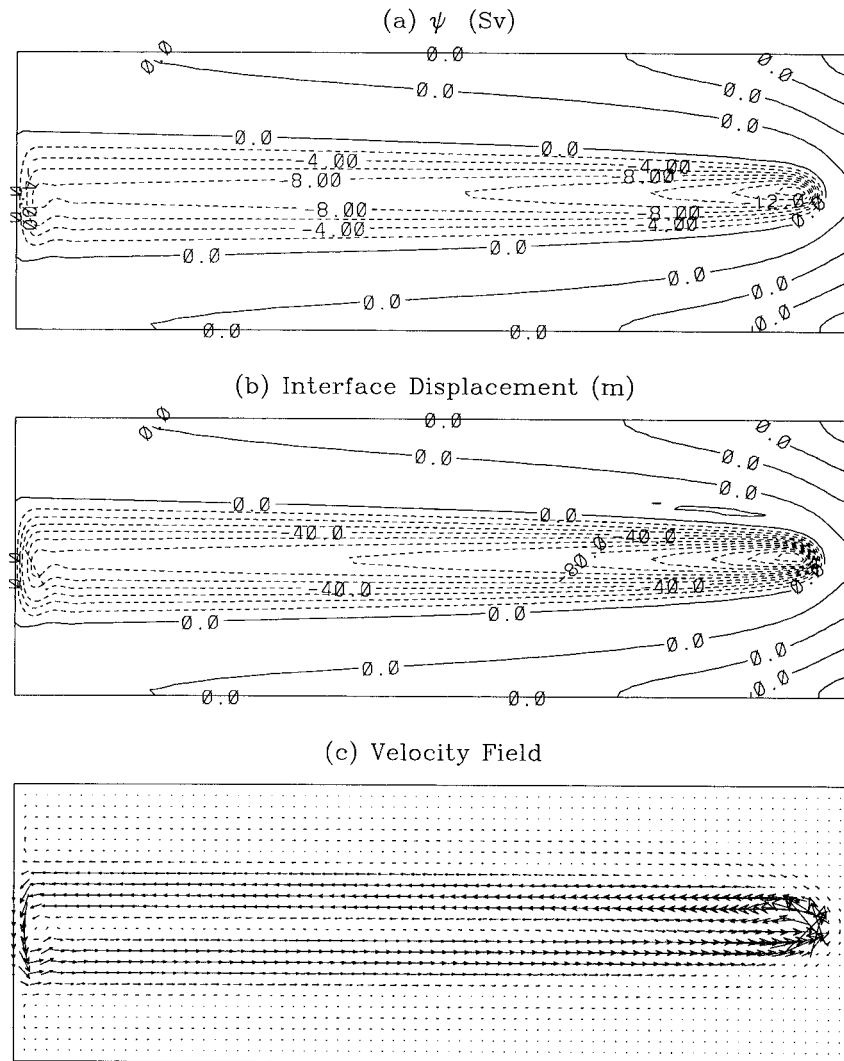


FIG. 5. Steady-state solution for QG simulation (expt A2) with model setup equivalent to that in expt A1. (a) Transport streamfunction (CI = 2 Sv), (b) interface displacement (CI = 10 m), and (c) velocity field (scaled the same as in Fig. 4c).

cause of the strong lateral shears in the zonal flows, especially when the source area is small (there is no baroclinic instability in a  $1\frac{1}{2}$ -layer model). Experiments A1 and A2 were conducted with low horizontal resolution (40 km) and with high eddy viscosity ( $\nu = 1000 \text{ m}^2 \text{ s}^{-1}$ ) such that the resulting flow patterns are steady in time.

In order to investigate how instabilities affect the nature of the circulation, a higher resolution (10 km) and much lower viscosity ( $\nu = 50 \text{ m}^2 \text{ s}^{-1}$ ) simulation, experiment A3, was conducted. The other parameters are identical to those in experiments A1 and A2. The sinking takes place over 16 grid points (instead of 1 grid point), preserving the sink's area and entrainment velocity as in the previous experiments. The flow is decomposed into a mean and an eddy component,  $\psi = \bar{\psi} + \psi'$ , and the mean flow is calculated in the usual way:

$\bar{\psi} = T^{-1} \int_{t_0}^{t_0+T} \psi dt$ , where  $t_0$  is the time at which the system reaches a statistically steady state (e.g., after a parameter change), and the averaging period  $T$  is large compared to the period of turbulent fluctuations such that  $\overline{\psi'} \approx 0$ . For experiment A3, the averaging period  $T$  is 5 years after a spinup period  $t_0$  of 10 years.

As soon as the flow becomes unstable, the circulation rapidly exhibits complicated patterns, as shown in Fig. 6a in an instantaneous plot of the transport streamfunction. The time-mean circulation (Fig. 6b), however, retains the structure of that in the lower resolution experiment A2 (Fig. 5a). Differences include a narrower circulation near the sink and a small asymmetry between the westward and eastward jets. The circulation is narrower near the sink due to the decrease in viscosity and wider elsewhere as a composite of the westward propagating eddies (Fig. 6a). We attribute the small asym-

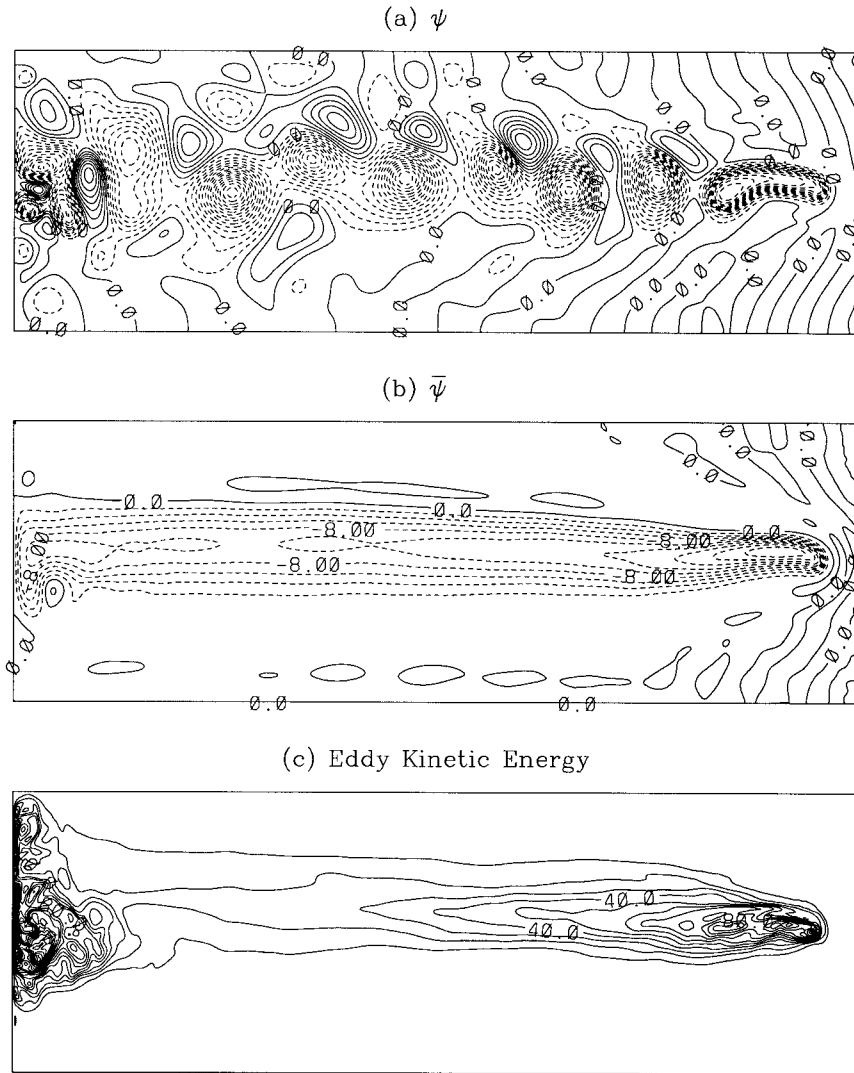


FIG. 6. (a) Instantaneous transport streamfunction (CI = 2 Sv), (b) mean transport streamfunction (CI = 2 Sv), and (c) eddy kinetic energy distribution (CI =  $10 \text{ cm}^2 \text{ s}^{-2}$ ) for high-resolution (10 km) QG simulation (expt A3).

metry between westward and eastward mean flows to the westward translation of the cyclonic eddies, which increases (decreases) the velocities in the northern (southern) jet. The return flow along the boundary current displays a more pronounced meander, probably associated with an arrested Rossby wave pattern (e.g., Moore 1963). The distribution of fluctuating motion is illustrated by plotting the eddy kinetic energy distribution ( $\text{EKE} = |\nabla\psi'|^2/2$ ) in Fig. 6c. The EKE distribution exhibits a north–south asymmetry, which can be related to the fact that the eddies tend to be more easily entrained into the westward jet than into the eastward jet as they migrate westward due to the  $\beta$  effect. The strong EKE signature near the western boundary illustrates fluctuations as the eddies interact with the western wall. The primary message of experiment A3 is that the

mean circulation pattern discussed in section 2 and obtained in experiments A1 and A2 remains quite robust in the eddy-resolving case A3.

#### 4. Impact of a localized sink on midlatitude ocean circulation

The results presented in the previous section imply that a localized sink near the eastern boundary of an ocean basin can generate recirculating flows in the upper ocean, which may in turn be strong enough to significantly alter the wind-driven circulation. In order to explore this issue, an idealized midlatitude ocean circulation is considered, driven both by wind forcing and a “thermohaline” flow. The following set of numerical experiments should be viewed as a process study and a

TABLE 3. Common parameters of the numerical simulations B1–B18.

Basin size ( $x, y$ )	7000 km $\times$ 2000 km
Coriolis parameters	$f_0 = 7.3 \times 10^{-5} \text{ s}^{-1}$ $\beta = 2 \times 10^{-11} \text{ m}^{-1} \text{ s}^{-1}$
Layer thickness	$H = 1000 \text{ m}$
Reduced gravity	$g' = 0.01 \text{ m s}^{-2}$
Deformation radius	$R_d = 42 \text{ km}$
Interfacial friction	$r = 5 \times 10^{-8} \text{ s}^{-1}$
Eddy viscosity	$\nu = 200 \text{ m}^2 \text{ s}^{-1}$ or $\nu = 50 \text{ m}^2 \text{ s}^{-1}$ ; see Table 4
Horizontal grid scale	20 km or 10 km; see Table 4

sensitivity analysis rather than as an attempt to simulate a realistic North Atlantic circulation.

### a. Model configuration

The domain is slightly wider zonally (7000 km) than the one used in the previous section and extends approximately from  $80^\circ$  to  $10^\circ\text{W}$ . The meridional extent is unchanged (2000 km) and the domain is centered at  $30^\circ\text{N}$ . As before, the mean depth of the active layer is 1000 m and the stratification is such that the radius of deformation is approximately 42 km. The experiments are conducted using grid spacings of 20 and 10 km, which resolve the mesoscale eddy activity. The idealized shape of the western boundary is chosen to represent the abrupt change of the coastline orientation at approximately  $35^\circ\text{N}$  associated with Cape Hatteras, which is thought to play an essential role in the inertial separation of the Gulf Stream (Dengg 1993; Özgökmen et al. 1997). Similarly, the eastern coastline is a crude representation of the African coast and the Gulf of Cadiz. There is no flow through the western and eastern boundaries. No-slip boundary conditions are applied along the western and eastern boundaries in the majority of experiments. Based on the sensitivity study by Verron and Blayo (1996), we employ a finite difference approximation developed by Woods (1954) to implement the no-slip boundary conditions. The northern boundary is closed from  $80^\circ$  to  $51^\circ\text{W}$  to represent the northeastern American coastline, but is open from  $51^\circ\text{W}$  to the eastern boundary. The southern boundary is open between the western and eastern walls. We have experimented with a variety of open boundary conditions [for a systematic analysis, see Chapman (1985)]. The mean circulation patterns are, however, quite insensitive to the open boundary conditions choice. In the experiments presented here, the explicit radiation condition of Orlandi (1976) was adopted. The model parameters are summarized in Table 3.

A thermohaline flow is imposed into and out of the model domain by modifying the potential vorticity equation (8) as

$$\frac{\partial q}{\partial t} + J(\psi, q) = \frac{f_0}{H}(w_E + w_S) + \nu \nabla^4 \psi - r \nabla^2 \psi - k_{\text{in,out}}(\nabla^2 \psi - \nabla^2 \psi_{\text{in,out}}^*), \quad (10)$$

where  $k_{\text{in,out}}$  are the relaxation coefficients and  $\psi_{\text{in,out}}^*$  are the flow profiles toward which the prognostic flow is forced at the inlet and outlet regions.

The inlet flow has the Munk profile given in terms of the relative vorticity distribution as

$$\nabla^2 \psi_{\text{in}}^* = \frac{\psi^T}{\delta^2} \exp\left(-\frac{x}{2\delta}\right) \left[ \cos\left(\frac{\sqrt{3}}{2} \frac{x}{\delta}\right) - \frac{1}{\sqrt{3}} \sin\left(\frac{\sqrt{3}}{2} \frac{x}{\delta}\right) \right], \quad (11)$$

where  $x$  is the zonal distance from the western wall,  $\delta = (\nu/\beta)^{1/3}$  is the scale of the viscous layer, and  $\psi^T$  is the strength of the thermohaline flow, taken as approximately 15 Sv. The inlet relaxation coefficient  $k_{\text{in}}$  decays exponentially from a maximum of  $(7 \text{ days})^{-1}$  to zero over a meridional distance of 200 km near the southwest corner of the domain (Fig. 7a). The outflow has a sinusoidal flow profile specified by the relative vorticity distribution

$$\nabla^2 \psi_{\text{out}}^* = \psi^T \left( \frac{\pi}{x_2 - x_1} \right)^2 \cos\left( \pi \frac{x' - x_1}{x_2 - x_1} \right), \quad (12)$$

where  $x' \geq x_1$ ,  $x_2 \geq x_1$ ,  $x'$  is the distance measured eastward from  $51^\circ\text{W}$  along the open northern boundary, and  $x_2 - x_1$  is the width of the outflow region (Fig. 7a), taken as 400 km. The outflow relaxation coefficient  $k_{\text{out}}$  decays from a maximum of  $(30 \text{ days})^{-1}$  to zero over a distance of 200 km. The model results show no significant sensitivity to the outflow conditions.

In addition to this thermohaline flow, which passes through the domain, there is also a flow induced by wind forcing, that recirculates within the domain. The wind forcing is steady in time and the Ekman pumping velocity (proportional to the wind stress curl) used in these simulations is depicted in Fig. 7b. The anticyclonic forcing is such that it generates a western boundary transport of approximately 20 Sv. A wind-induced western boundary transport of 20 Sv and a thermohaline transport of 15 Sv are in approximate agreement with the observed values in the North Atlantic Ocean (Schmitz et al. 1992). A cyclonic wind forcing is also applied to the north of the approximate observed path of the Gulf Stream (Fig. 7b). While this feature is present to some extent in all available wind stress climatologies (e.g., Townsend et al. 2000), the magnitude of the forcing applied here is higher than realistic values. This facilitates the separation of the model Gulf Stream from the coastline at  $35^\circ\text{N}$  [see related discussion in Özgökmen et al. (1997)]. Finally, a small interfacial drag coefficient of  $r = 5 \times 10^{-8} \text{ s}^{-1}$  is applied to stabilize the meanders of the model Gulf Stream. This is consistent with the observational evidence of Weatherly (1984), who concluded that for the observed Gulf Stream, most of the dissipation takes place by bottom friction in the region of the meanders after the jet's separation from the coast, rather than by lateral friction along the western boundary. The characteristics of the

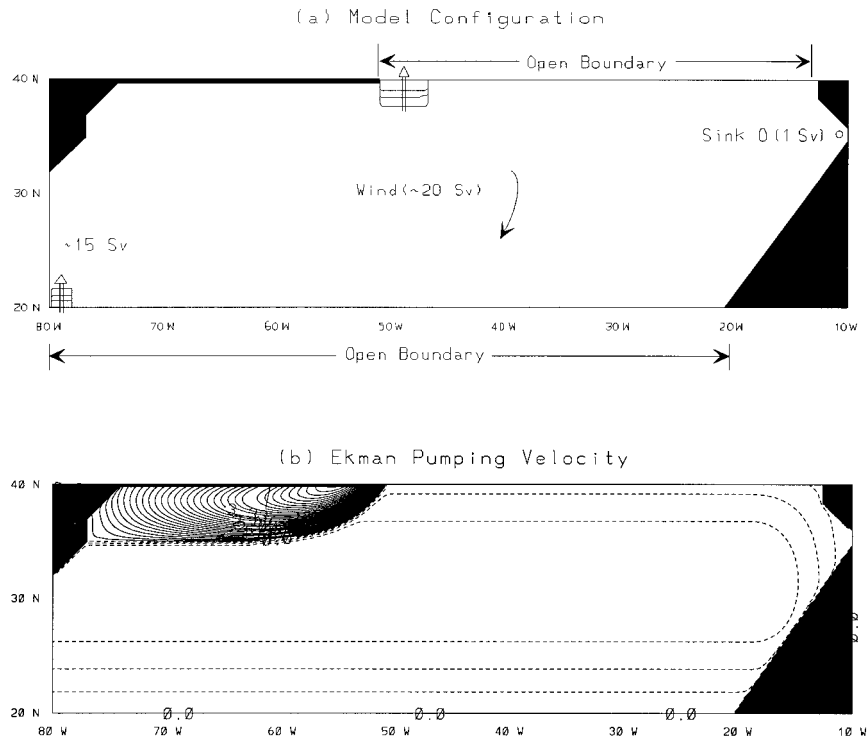


FIG. 7. (a) Schematic illustration of the model configuration showing eastern and western coastlines, southern and northern open boundaries, and the locations of the inflow/outflow regions. (b) The Ekman pumping velocity  $w_E$  ( $CI = 0.2 \times 10^{-6} \text{ m s}^{-1}$ ).

sensitivity experiments discussed in the following section are summarized in Table 4.

*b. Numerical experiments*

1) THE WIND- AND THERMOHALINE-DRIVEN CIRCULATION (NO SINK)

The first experiment, denoted B1, is conducted without any sink near the eastern boundary. After a spinup phase of 20 years, a mean flow field is calculated over the following 5 years. The results are presented in Fig.

TABLE 4. List of numerical experiments described in section 4b.

Expt	Sink intensity	Characteristics
B1	0	Without sink
B2	1.0 Sv	Reference experiment
B3	0.5 Sv	Reduced sink strength
B4	2.0 Sv	Increased sink strength
B5	1.0 Sv	Distributed sink
B6	1.0 Sv	Free slip eastern boundary condition
B7	1.0 Sv	Sink location moved westward
B8	1.0 Sv	Steeper eastern coastline
B9	1.0 Sv	Higher resolution (10 km, $\nu = 50 \text{ m}^2 \text{ s}^{-1}$ )
B10–B16	1.0 Sv	Sink's distance from the boundary is varied (high resolution)
B17	0	Local wind forcing over the sink
B18	1.0 Sv	Local wind forcing over the sink

8. The 35-Sv western boundary current flows along the boundary until the sharp turn of the coastline at 35°N where it separates from the coast. The free midlatitude jet then meanders and generates eddies, which then act as a downgradient flux of potential vorticity (Rhines and Young 1982) and form recirculating flows on both flanks of the jet (Hogg and Johns 1995). The jet's transport increases several times over that of the western boundary current to approximately 75–80 Sv [in reasonable agreement with observations (Schmitz and McCartney 1993)]. The net northward transport of 15 Sv imposed across the domain (i.e.,  $\psi = 0$  at the western boundary and  $\psi = 15 \text{ Sv}$  at the eastern boundary) as the thermohaline component exits the domain at the northern boundary as a narrow current, an idealized representation of the North Atlantic Current.

2) SENSITIVITY OF THE CIRCULATION TO THE SINK INTENSITY

A sink is placed near the eastern boundary (Fig. 9), representing entrainment of the active layer fluid at a rate of 1 Sv through one grid point (the velocity scale is  $2.5 \times 10^{-3} \text{ m s}^{-1}$ ). This is an idealized representation of the localized entrainment that takes place over a small distance of approximately 40–50 km (Baringer and Price 1997b; their Fig. 7a). The results of this experiment (B2) are depicted in Fig. 10a. A pronounced cy-

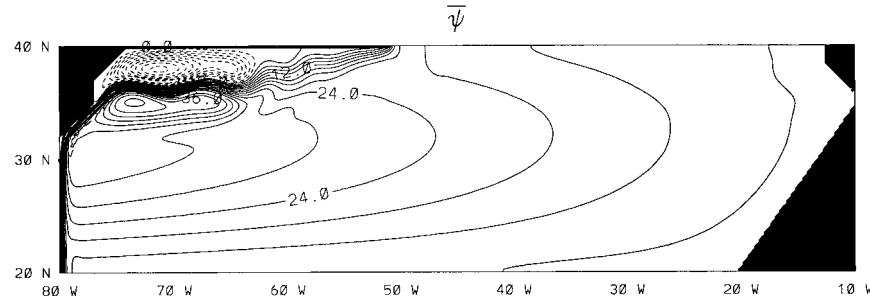


FIG. 8. Mean transport streamfunction ( $CI = 3 \text{ Sv}$ ) for experiment B1, which does not include the sink.

clonic circulation develops near the eastern boundary, which elongates westward and distorts the contours of the wind-driven flow. The effect of this circulation extends all the way to the model Gulf Stream region (approximately  $65^\circ\text{W}$ ) and leads to the bifurcation of the jet to a northward flowing branch (as before) and an eastward flowing branch (cf. Figs. 8 and 10a). For a standard documentation of this feature, the transport and zonal velocity are plotted along the meridional section at  $30^\circ\text{W}$  (Figs. 11a,b). This longitude is selected in order to best capture a model AzC (e.g., see Figs. 2a,b). The strength of the eastward flowing branch in experiment B2 is approximately  $6.8 \text{ Sv}$ . The eastward current is located between  $32^\circ$  and  $35^\circ\text{N}$ , with zonal velocities reaching  $15 \text{ cm s}^{-1}$ . Hence, its location is consistent with that of the AzC, but its transport is weaker. There is also a countercurrent due to the nature of the circulation associated with an isolated sink, as discussed in sections 2 and 3. With a transport of  $4.3 \text{ Sv}$  and a westward zonal velocity of  $9 \text{ cm s}^{-1}$ , the countercurrent is weaker than its eastward counterpart. This difference is mostly due to the wind-driven background flow (Fig. 11). From now on, we will refer to the modeled eastward

current as  $AzC^*$  and to the modeled westward current as  $AzCC^*$ . The notations  $AzC$  and  $AzCC$  will be used for the observed Azores Current and Countercurrent (see section 5 for a detailed discussion of the latter), respectively.

Two additional experiments were conducted to investigate the sensitivity of these currents to the intensity of the sink. While the latest estimates of the entrainment are on the order of  $1 \text{ Sv}$  (e.g., Baringer and Price 1997a), higher rates have been reported [up to  $5.5 \text{ Sv}$  by Howe (1984)]. In experiment B3, the sink strength is decreased to  $0.5 \text{ Sv}$  (by reducing the velocity scale to  $1.25 \times 10^{-3} \text{ m s}^{-1}$ ), and in experiment B4 the strength of the sink is increased to  $2 \text{ Sv}$ . The results are shown in Figs. 10b and 10c, respectively. The transport of the  $AzC^*$  ( $AzCC^*$ ) in experiment B3 reduces to  $3.8 \text{ Sv}$  ( $1.5 \text{ Sv}$ ), and the maximum zonal velocity to  $8 \text{ cm s}^{-1}$  ( $-4 \text{ cm s}^{-1}$ ). (Fig. 11). In experiment B4, a far stronger effect of the sink is apparent with respect to that in B1 and B2, since the mean path of the model Gulf Stream is shifted to the south by approximately  $100 \text{ km}$  (compare Figs. 8 and 10c). The transport of the  $AzC^*$  ( $AzCC^*$ ) in experiment B4 increases to  $12.1 \text{ Sv}$  ( $9.4 \text{ Sv}$ ), and the maximum zonal velocity to  $27 \text{ cm s}^{-1}$  ( $-22 \text{ cm s}^{-1}$ ). Not too surprisingly, experiments B2–B4 indicate that the sink has a stronger impact on the general circulation (Fig. 10) when its intensity is greater. There is a quasi-linear relationship between the velocity and transport of the  $AzC^*$  (Fig. 11) and the sink strength. The values of the transports and zonal velocities of the  $AzC^*$  and  $AzCC^*$  at  $30^\circ\text{W}$  are tabulated in Table 5 for each experiment.

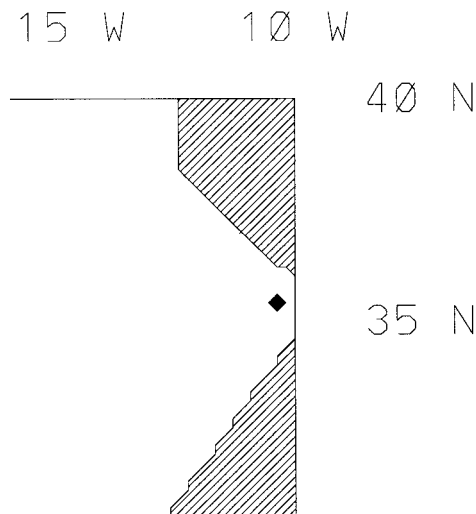


FIG. 9. Sink location in experiments B2–B4, B6–B8, and B18.

### 3) IMPACT OF SINK DISTRIBUTION

In order to determine the consequences of the idealization of entrainment as a delta-function on the large-scale circulation pattern, the entrainment distribution was modified in experiment B5. In this experiment, the total entrainment volume flux of  $1 \text{ Sv}$  is preserved, but both the velocity scale and the entrained distance are modified. The entrainment velocity  $w_s$  of about  $3.6 \times 10^{-4} \text{ m s}^{-1}$  is distributed over seven grid points forming a strip of  $140 \text{ km}$  (roughly the length of the Mediter-

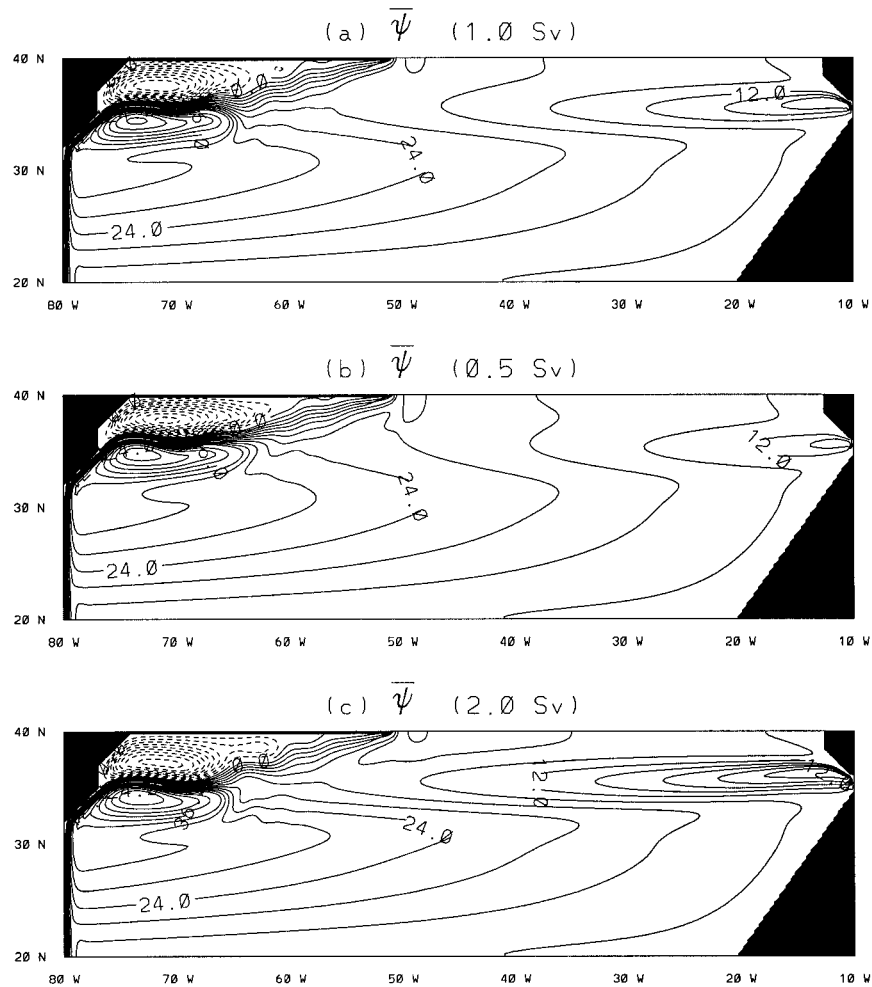


FIG. 10. Mean transport streamfunctions ( $CI = 3 \text{ Sv}$ ) for experiments (a) B2, (b) B3, and (c) B4, which include sinks with intensities of 1.0, 0.5, and 2.0 Sv near the eastern boundary, respectively.

ranean overflow)  $\times 20 \text{ km}$  (the size of the grid spacing) equidistant from the coastline (Fig. 12). The resulting upper-ocean circulation is shown in Fig. 13a. It is not significantly different from that of experiment B2 with the Dirac-delta distribution (Fig. 10a), except in the close vicinity of the sink. The transport of the AzCC\* ( $AzCC^*$ ) at  $30^\circ\text{W}$  increases by 22% (28%) to 8.3 Sv (5.5 Sv). A similar increase is obtained for the zonal velocity (Figs. 13b,c; Table 5). This result indicates that the large-scale circulation patterns do not appear to be very sensitive to the details of the entrainment distribution. The induced large-scale circulation is, however, strongly dependent on how close the sink is to the coastline [see section 4b(6) for details].

#### 4) IMPACT OF THE EASTERN BOUNDARY

In view of the proximity of the sink location to the eastern boundary (Fig. 9), we investigate whether or not the eastern boundary condition and coastline shape have

any impact on the resulting circulation. In experiment B6, the boundary condition along the eastern boundary is changed from no-slip to free-slip. In the results of this experiment (not shown), the cyclonic circulation generated by the sink follows the eastern coastline more closely than in the no-slip experiment (Fig. 10), where the AzCC\* tends to separate earlier from the eastern coastline with a smaller meridional extent for the cyclonic circulation. This is consistent with the well-known difference between free-slip and no-slip boundaries (e.g., Boudra and Chassignet 1988; Chassignet and Gent 1991; Haidvogel et al. 1992). Also, due to the lack of a viscous sublayer at the free-slip wall, the energy dissipation decreases with respect to that of a no-slip wall (experiment B2), and the transport of the AzCC\* ( $AzCC^*$ ) at  $30^\circ\text{W}$  becomes 8.6 Sv (5.5 Sv) with an increase in the maximum zonal velocity to  $17 \text{ cm s}^{-1}$  ( $-12 \text{ cm s}^{-1}$ ) (Table 5).

The role of boundary layer dissipation was further analyzed by moving the location of the sink westward

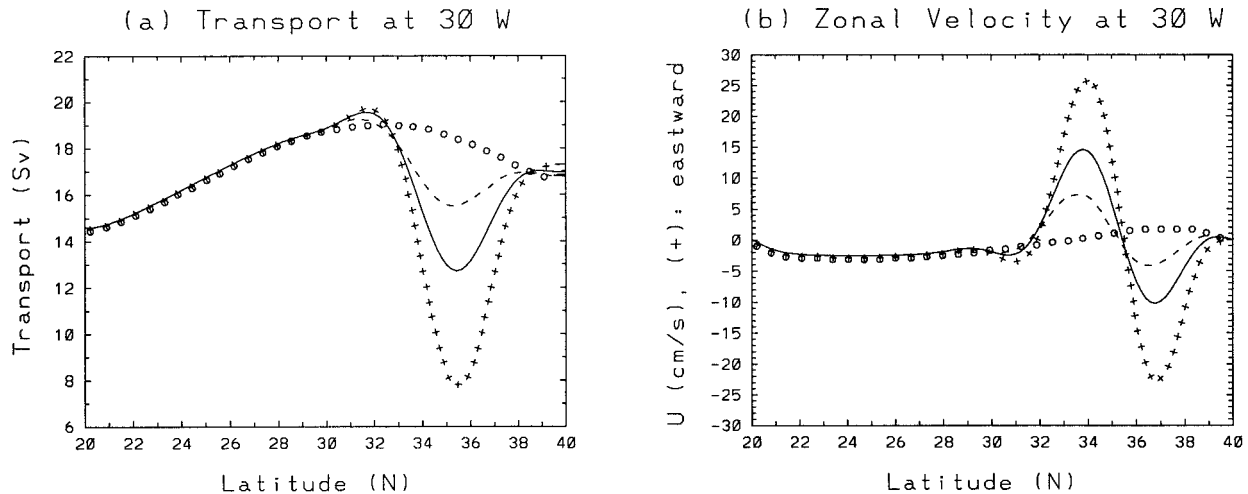


FIG. 11. (a) Mean transport streamfunctions (in Sv) along the meridional cross section at 30°W, and (b) zonal velocities (in  $\text{cm s}^{-1}$ , positive eastward) at 30°W, for experiments B1 [no sink, lines with (o)], B2 [1.0 Sv sink, solid lines], B3 [0.5 Sv sink, lines with (-)], and B4 [2.0 Sv sink, lines with (+)].

by one grid space (20 km) with respect to that shown in Fig. 9. As anticipated, this leads to less interaction of the cyclonic circulation with the boundary, since it remains outside of the viscous sublayer, whose thickness is on the order of one grid space ( $\delta = 21.6 \text{ km}$  for  $\nu = 200 \text{ m}^2 \text{ s}^{-1}$ ). Consequently, the cyclonic circulation intensifies in experiment B7 (not shown), in which the transport of the AzC\* (AzCC\*) at 30°W becomes 10.4 Sv (7.7 Sv), and the maximum zonal velocity reaches  $23 \text{ cm s}^{-1}$  ( $-17 \text{ cm s}^{-1}$ ) (Table 5).

Finally, in order to investigate the sensitivity of the circulation to the shape of the coastline in the vicinity of the sink, the angle of the modeled Gulf of Cadiz was modified to generate a steeper (with respect to the  $y$  axis) boundary in experiment B8. The resulting circulation (not shown) reveals no significant change in the large-scale circulation pattern or in the transport of the AzC\* (Table 5).

TABLE 5. Transport and maximum zonal velocity of the eastward (AzC\*) and westward (AzCC\*) currents at 30°W in experiments B1–B9, B17–B18.

Expt	AzC*		AzCC*	
	Transport (Sv)	U ( $\text{cm s}^{-1}$ )	Transport (Sv)	U ( $\text{cm s}^{-1}$ )
B1	—	—	—	—
B2	6.8	15	4.3	-9
B3	3.8	8	1.5	-4
B4	12.1	27	9.4	-22
B5	8.3	18	5.5	-11
B6	8.6	17	5.5	-12
B7	10.4	23	7.7	-17
B8	5.7	13	3.5	-8
B9	8.0	15	5.6	-12
B17	2.2	4	—	—
B18	8.3	18	6.0	-13

## 5) IMPACT OF HORIZONTAL RESOLUTION

The impact of higher horizontal resolution is investigated in experiment B10, with a grid spacing of 10 km and eddy viscosity  $\nu = 50 \text{ m}^2 \text{ s}^{-1}$ . The sink distribution differs from that depicted in Fig. 12 in that the width of the strip is reduced to 10 km and that it is distributed over 14 grid points. The length is still 140 km, and the entrainment velocity scale at each grid point is approximately  $7.2 \times 10^{-4} \text{ m s}^{-1}$ , so that the total entrainment volume flux is maintained at 1 Sv.

The mean transport streamfunction in experiment B9 is illustrated in Fig. 14a. One of the main differences from experiment B5 (Fig. 13a) is that the model Gulf Stream penetrates into the open ocean farther as a coherent jet in B9. The bifurcation of the model Gulf

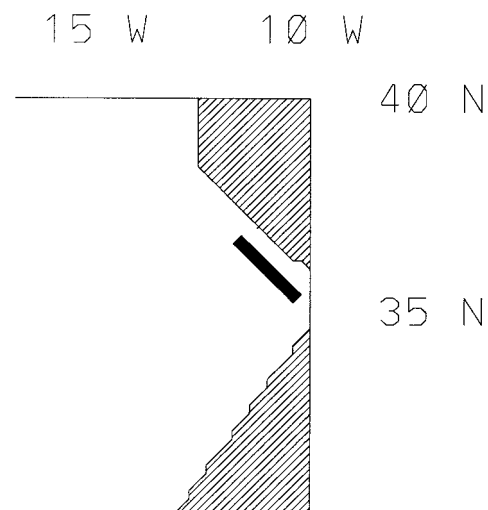


FIG. 12. Sink distribution in experiment B5.

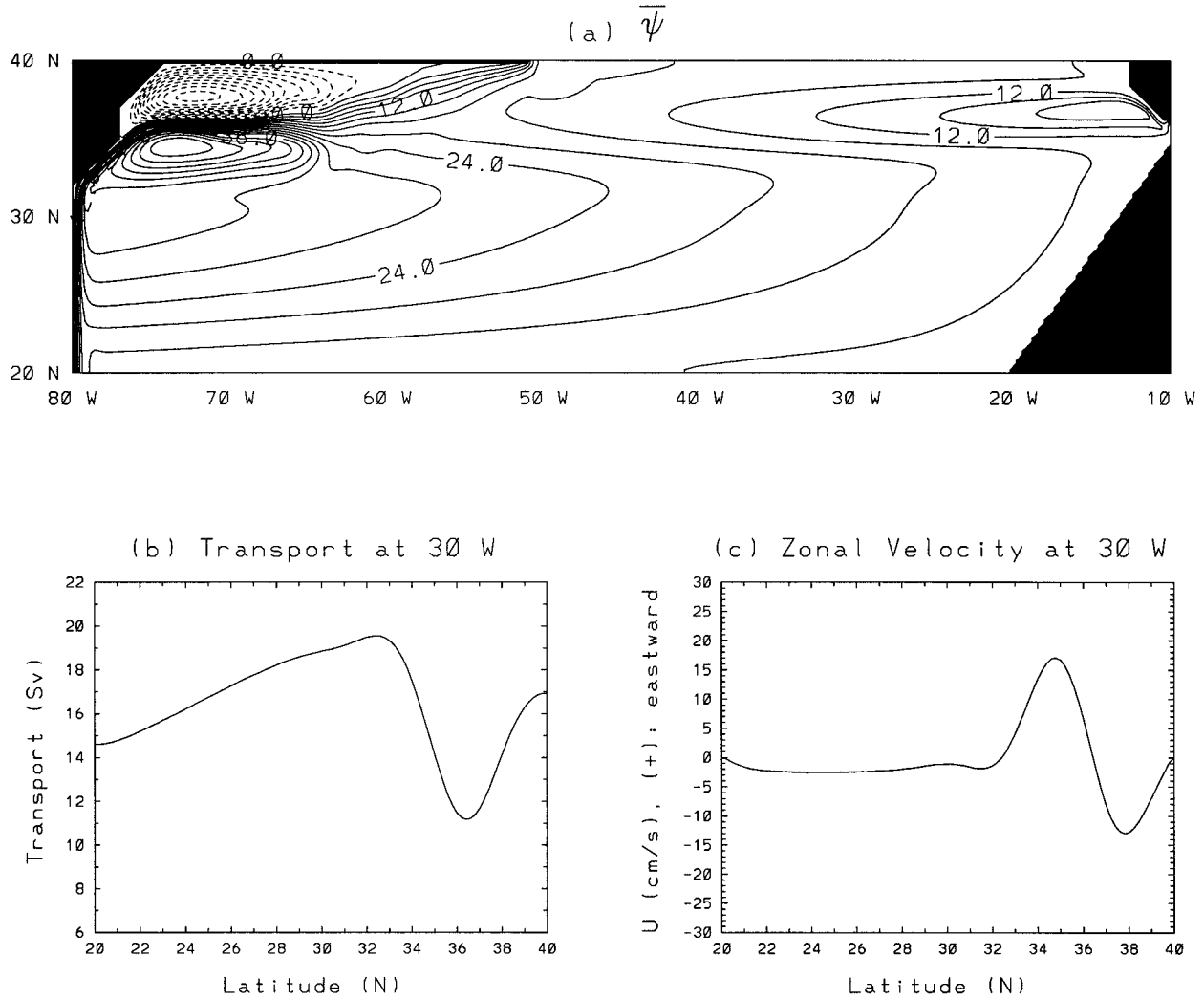


FIG. 13. (a) Mean transport streamfunction (CI = 3 Sv), (b) mean transport streamfunction along the meridional cross section at 30°W, and (c) zonal velocity (in  $\text{cm s}^{-1}$ , positive eastward) at 30°W, for experiment B5, where the sink distribution corresponds to that depicted in Fig. 12.

Stream into the model North Atlantic Current and the AzC\* takes place at almost 50°W in the higher resolution experiment, as opposed to approximately 65°W in the lower resolution experiment. This behavior is consistent with the well-investigated dynamics of jet penetration in this parameter range (e.g., Holland and Schmitz 1985; Barnier et al. 1991; Chassignet and Gent 1991). On the eastern side of the basin, the basic structure of the AzC\* and AzCC\* are qualitatively and quantitatively similar, with some differences near the sink region. The transport of the AzC\* (AzCC\*) at 30°W is 8.0 Sv (5.6 Sv) in B9 versus 8.3 Sv (5.5 Sv) in B5, and the maximum zonal velocity is 15  $\text{cm s}^{-1}$  (–12  $\text{cm s}^{-1}$ ) in B9 versus 18  $\text{cm s}^{-1}$  (–11  $\text{cm s}^{-1}$ ) in B5 (Table 5). This result further supports the conclusion of section 4b(3) that for localized sinks, the details of the sink distribution are less important for the large-scale circulation than the total amount of volume transfer.

While the mean circulation fields are quite similar, significant differences are found between the high-resolution experiment B9 and the low-resolution experiments in the variability of the circulation. The fronts associated with the AzC\* and the AzCC\* are stable in time in the experiments conducted with 20-km resolution, whereas they become unstable and consist typically of cyclonic eddies that migrate westward in the higher resolution (and lower viscosity) experiment, as depicted in an instantaneous transport streamfunction plot during the statistically steady state (Fig. 14b). The eddy activity is less vigorous when compared with that shown in Fig. 6a for a sink alone, due to the interaction of the circulation with the eastern boundary and also with the wind-driven circulation. Beckmann et al. (1994, and references therein) report that the EKE associated with the Azores frontal zone averaged between 28° and 32°W approaches 200  $\text{cm}^2 \text{ s}^{-2}$  according to satellite and drifter

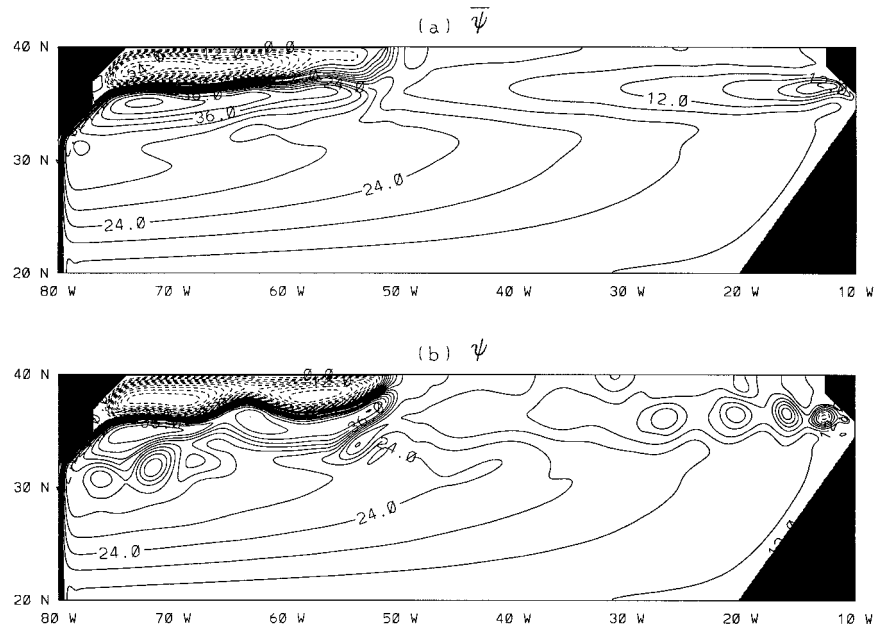


FIG. 14. (a) Mean transport streamfunction and (b) instantaneous transport streamfunction (CI = 3 Sv) for high-resolution experiment B9, where the grid spacing is reduced to 10 km and eddy viscosity to  $50 \text{ m}^2 \text{ s}^{-1}$ .

measurements, and propose baroclinic instability as the primary mode of instability of the Azores frontal zone. In the present numerical model, only barotropic instabilities can arise, and the EKE level (not shown) is an order of magnitude lower in experiment B9 than in the observations.

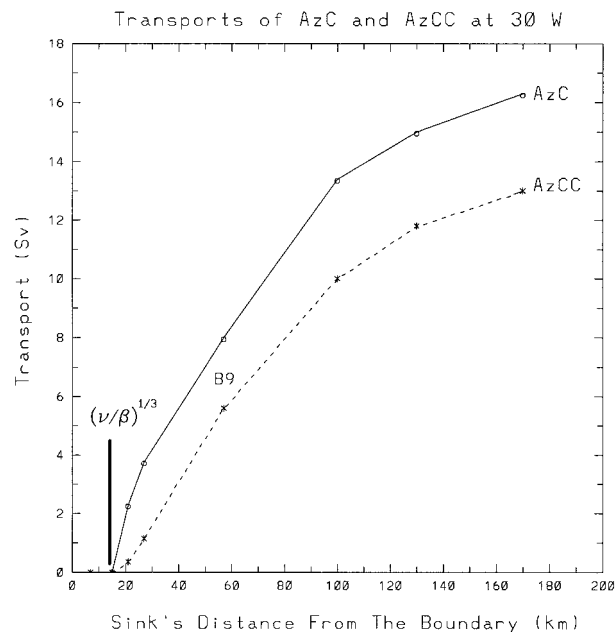


FIG. 15. Zonal transports of AzC\* and AzCC\* at  $30^\circ\text{W}$  as a function of the sink's distance from the coastline in experiments B9–B16. The circles and stars mark the data points, and the thick solid line shows the viscous boundary layer thickness.

#### 6) IMPACT OF THE COASTLINE'S PROXIMITY

Frictional effects can become a leading term in the potential vorticity budget when the vertical motions are confined to small areas on the order of viscous boundary layer thickness and are adjacent to the boundary (Spall 2000). An increase of more than 25% in the transports of the currents was observed in B7 when the sink's location was moved westward by 1 grid point (20 km). In order to quantify the impact of the coastline's proximity on the induced circulation, seven high-resolution (10 km) experiments (B10–B16) are conducted. In these experiments, the sink's distance from the coastline is varied from 7 km (closest grid point to the coastline) to 170 km. The experiments are otherwise identical to experiment B9. The results are summarized in Fig. 15, which shows the zonal transports of the AzC\* and the AzCC\* at  $30^\circ\text{W}$  as a function of the sink's distance to the northern coastline (see Fig. 12). Figure 15 shows that when the sink's distance from the coastline is equal to or less than the viscous boundary layer thickness (approximately equal to 15 km in these experiments), the frictional forces almost entirely suppress the circulation induced by the sink. As the sink is moved away from the boundary, the magnitudes of the currents increase to reach approximately 16 and 13 Sv at  $30^\circ\text{W}$  for the AzC\* and AzCC\*, respectively, when the sink is located at a distance from the coastline approximately an order of magnitude larger than the viscous layer thickness. The primary reason for the difference in magnitude between the AzC\* and the AzCC\* in our experiments is the wind-driven circulation, which adds about 2.5 Sv to the AzC\* at  $30^\circ\text{W}$  (see Fig. 11a). This

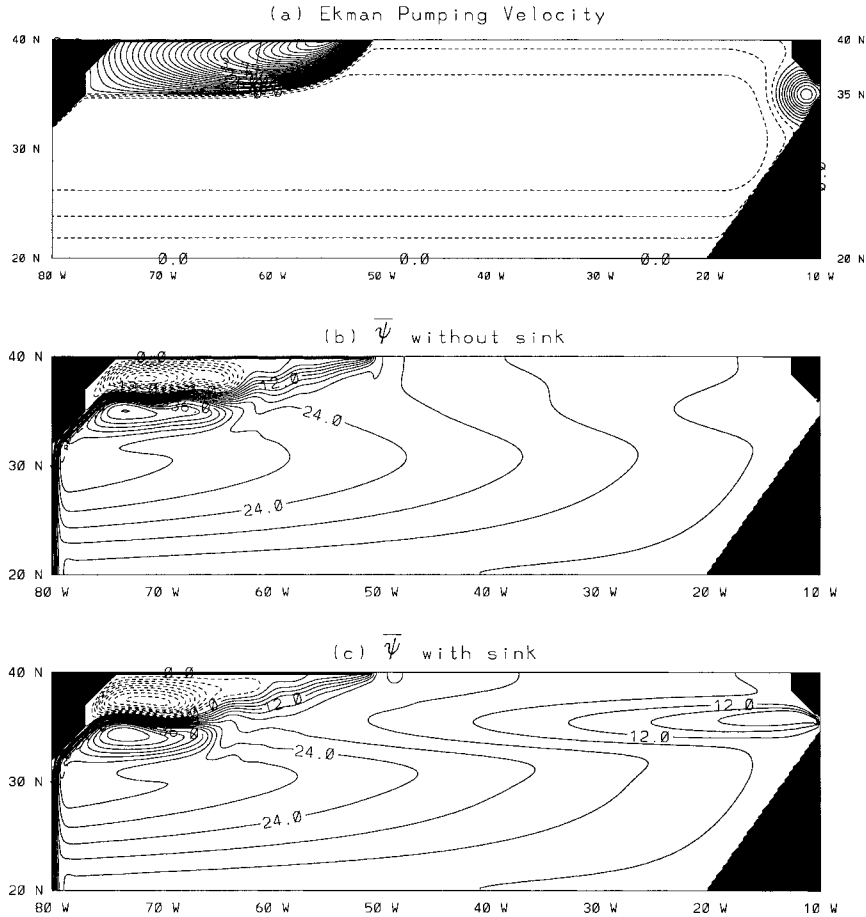


FIG. 16. (a) The Ekman pumping velocity  $w_E$  ( $CI = 0.2 \times 10^{-6} \text{ m s}^{-1}$ ) used in experiments B17 and B18. Note the positive values (cyclonic forcing) over the "gulf." Mean transport streamfunctions ( $CI = 3 \text{ Sv}$ ) for (b) experiment B17 (without sink) and (c) experiment B18, which contains a sink of 1 Sv near the eastern boundary.

series of experiments shows that the distance of the sink from the boundary strongly impacts the transports of the zonal currents.

#### 7) IMPACT OF LOCAL WIND FORCING

So far we have considered only the impact of a localized sink near the eastern boundary on the formation of the AzC\*. It is clear from (8) that Ekman pumping can also contribute via the identical (Sverdrup) dynamics, provided that suitable forcing exists in the region. Townsend et al. (2000) analyzed in detail 11 different wind stress climatologies most commonly available to the oceanographic community, and showed that 10 of these climatologies exhibit high cyclonic forcing ( $w_E > 0$ ) over the Gulf of Cadiz. In order to determine the importance of this forcing on the AzC\*, two numerical experiments (B17 and B18) were conducted.

The Ekman pumping velocity used in experiments B1–B9 (Fig. 7b) is modified to incorporate cyclonic wind forcing over the modeled Gulf of Cadiz (Fig. 16a),

where a positive Ekman pumping velocity  $w_E$  reaching  $2 \times 10^{-6} \text{ m s}^{-1}$  is applied both in B17 and in B18. The total Ekman convergence induced by this forcing is approximately 0.14 Sv, and it is therefore much less than the sink's contribution. The resulting circulation without the sink is illustrated in Fig. 16b (experiment B17). In comparison to experiment B1 (Fig. 8), the streamlines in B17 near the eastern boundary depict eastward and westward currents. At  $30^\circ\text{W}$ , the eastward current induced by this particular wind forcing transports 2.2 Sv zonally, in agreement with the results of Townsend et al. (2000), in which the transport values range from 0.70 to 4.25 Sv depending on the wind stress climatology used. The transport of the westward current is negligibly small at this longitude. When a sink of 1 Sv is included in experiment B18, the transport of the AzC\* (AzCC\*) at  $30^\circ\text{W}$  becomes 8.3 Sv (6.0 Sv), and the maximum zonal velocity reaches  $18 \text{ cm s}^{-1}$  ( $-13 \text{ cm s}^{-1}$ ) (Fig. 16c, Table 5). These values are higher with respect to those in experiment B2, which does not contain the cyclonic forcing over the modeled Gulf of Cadiz, due

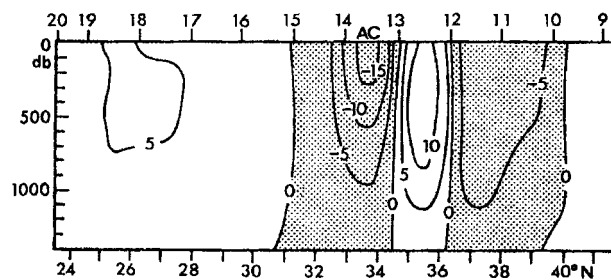


FIG. 17. Geostrophic velocity in  $\text{cm s}^{-1}$  (positive to the west) at  $23^\circ\text{W}$  in Nov 1988 reported by Rios et al. (1992).

to the increase in the vertical velocity in experiment B18 by the Ekman convergence. These experiments highlight the difference of the effect between strong localized (e.g., due to entrainment) forcing and weakly distributed (e.g., due to wind) forcing. Based on the above arguments, it appears that wind forcing alone cannot account for the entire transport of the AzC. It can, however, enhance its strength.

## 5. Discussion

A prominent feature in all simulations is the AzCC\* that, at  $30^\circ\text{W}$ , has a transport with magnitude 60%–70% of the corresponding AzC\* transport (Table 5). There is observational evidence for the existence of a counter-current just to the north of the AzC. Geostrophic velocities along a vertical section at  $23^\circ\text{W}$  by Rios et al. (1992) show an intense westward current band just north of the AzC (Fig. 17). A similar westward current is clearly visible also in the observations by Stramma and Müller (1989). Onken (1993) was the first to suggest the existence of a narrow band of westward transport in the eastern part the North Atlantic at about the Azores latitude. He postulated that the AzCC cannot be deduced directly at the surface, but rather is more pronounced in the 0–800 m layer. Onken (1993) attributed the existence of the AzCC to a feature in the meridional derivative of the wind stress curl. Recent observations by Cromwell et al. (1996), based on altimetry and hydrography, indicate that such westward flow north of the AzC appears to be a persistent feature of the circulation in this region. A recent study of climatological hydrographic data by Iorga and Lozier (1999a,b) shows the existence of a strong westward flow exiting the Gulf of Cadiz as well as a cyclonic circulation at approximately 1000-m depth centered in the Gulf. Additional evidence for the existence of the AzCC is provided by an inverse modeling study conducted by Mauritzen et al. (2000) using the hydrographic data at  $9^\circ\text{W}$  analyzed by Swallow (1969). The inverse model shows that more water enters eastward (about 7 Sv) than needed for the entrainment in the Gulf of Cadiz and the dense water formation in the Mediterranean Sea, that is, approximately 2 Sv. The remainder (about 5 Sv) is transported

westward via a northward recirculating boundary current in the Gulf. These features are consistent with the modeled circulation patterns presented in this paper.

In the numerical simulation of Chassignet et al. (2000, manuscript submitted to *J. Geophys. Res.*), the counter-current is clearly visible in the surface layer (Fig. 2a). A qualitatively similar cyclonic circulation is encountered also in the simulations by Jia (2000). In the experiments introduced in this paper, the signature of the AzCC\* is quite strong. Since the entrainment process takes place at a depth of approximately 1000 m, the surface signature of the eastward and westward jet may differ in the case of a continuously stratified fluid. For instance, a westward jet is more susceptible to becoming baroclinically unstable, a process not represented in our idealized experiments. Other effects such as the fluid exchange with the Mediterranean Sea through the Straits of Gibraltar [leading to a ventilation process discussed by Pedlosky (1983)] may also be of importance. Finally, we note the possible role of topographic effects; the Horseshoe Seamounts near the Gulf of Cadiz exist in such a way that it is easier for an eastward jet located between  $32^\circ$  and  $35^\circ\text{N}$  to flow toward the Gulf of Cadiz than for a westward jet between  $36^\circ$  and  $38^\circ\text{N}$  to exit from the Gulf of Cadiz. Hence, topographic influences can be a possible cause of path deflection and/or instability. In summary, there is observational support of the existence of an AzCC in this region, whose location and direction can be explained by the mechanism that simultaneously leads to the formation of the AzC.

## 6. Summary and conclusions

The large-scale dynamical impact of the interaction between the Mediterranean overflow and the eastern subtropical Atlantic has been investigated in terms of the response of the upper-ocean circulation to a localized and steady potential vorticity source near the eastern boundary of the basin. This potential vorticity source is an idealized representation of the entrainment of the North Atlantic water into the Mediterranean outflow, as the latter sinks rapidly in the Gulf of Cadiz upon exiting the Gibraltar Strait. The motivation for this investigation was provided by a recent study by Jia (2000), who found a direct link between the emergence of an AzC in a realistic OGCM and the water mass transformations associated with the Mediterranean outflow in the Gulf of Cadiz. Simulations of the subtropical gyre with the same OGCM by Paiva et al. (2000) and Chassignet et al. (2000, manuscript submitted to *J. Geophys. Res.*) also support this interpretation, despite the different resolutions and domain configurations.

Since the aforementioned OGCM studies indicate a cause and effect relationship between the formation of the AzC and the localized entrainment in the Gulf of Cadiz, we greatly reduced the complexity of the numerical model necessary to capture the essential dynamics. In this study, we employ a  $1\frac{1}{2}$ -layer quasigeo-

strophic model, in which the loss of fluid from the active layer is represented as a source of potential vorticity. The adequacy of the quasigeostrophic formulation is justified both by analytical arguments and by a comparison with a  $1\frac{1}{2}$ -layer primitive equation simulation with a similar setup, in which the divergent flow effects associated with a local upper-layer sink are explicitly represented. The dynamics investigated here are essentially the same as for the  $\beta$ -plume mechanism proposed by Stommel (1982) as an explanation for the westward extended chemical signature in the Pacific Ocean. The upper-ocean cyclonic eddy generated by the loss of mass over a localized area elongates westward under the influence of the  $\beta$  effect until the flow encounters the western boundary. In the steady state, the circulation pattern consists of bidirectional zonal flows with a limited meridional extent, as described by Pedlosky (1996). In the numerical experiments presented in this paper, the recirculating flows sustain a transport whose intensity is an order of magnitude higher than that of the sink.

A series of parameter sensitivity experiments were then conducted to explore the relevance of this sink-induced circulation pattern to the AzC. These experiments were performed in the context of an idealized midlatitude circulation, driven both by wind forcing and thermohaline flow through the open southern and northern boundaries. It is shown that the sink can significantly alter the upper-ocean flow and induce a zonal eastward current, to the south of the sink location ( $\sim 35^\circ\text{N}$ ), which resembles the AzC. This mechanism also generates a westward current to the north of the sink location. The existence of an AzCC was initially proposed by Onken (1993) and has been observed to be a persistent oceanic feature to the north of the AzC (Cromwell et al. 1996). Further observational support for the AzCC is provided by a recent climatological investigation of historical data (Iorga and Lozier 1999a,b) that show a westward flow exiting the Gulf of Cadiz and a cyclonic circulation at 1000-m depth centered in the Gulf. Using an inverse model on data collected along  $9^\circ\text{W}$ , Mauritzen et al. (2000) show that more water enters eastward the Gulf of Cadiz than needed for the entrainment and the dense water formation in the Mediterranean Sea, and that the remainder is transported westward. The  $\beta$ -plume mechanism investigated in the present study therefore addresses both the location and direction of the zonal current system associated with the AzC and AzCC. While this mechanism may not be the only factor important for the dynamics of this current system, it is likely to be a major factor in controlling the location of the AzC; a recent analysis of Geosat altimeter data (Le Traon and De Mey 1994) indicates no significant interannual shift in the mean zonal axis of the AzC.

Additional experiments were carried out to determine the sensitivity of these currents to various factors: boundary layer processes, sink intensity, sink distribution, model resolution, proximity of the sink to the

coastline, and local wind forcing. The transports of the currents are found to be sensitive to two main factors: the sink intensity and the distance of the sink from the coastline. A quasi-linear increase in transport of the AzC\* is obtained in the present model as a function of the sink strength. The transports of the AzC\* and the AzCC\* are strongly affected by frictional processes when the sink is positioned near the coastline, within a distance on the order of the viscous boundary layer thickness. In OGCMs, one can expect the AzC\*–AzCC\* system to be quite sensitive to the details of the entrainment process.

The results of this study support the idea of a possible link between the Mediterranean outflow processes and the formation of zonal currents in the North Atlantic upper-ocean circulation and emphasize the importance of the parameterization and representation of these processes in OGCMs.

*Acknowledgments.* T. M. Özgökmen and E. P. Chassignet greatly appreciate the support of National Science Foundation Grant OCE 9711186, and C. G. H. Rooth acknowledges institutional support from the University of Miami. We would like to thank B. Cushman-Roisin for insightful comments on an earlier version of this manuscript, Z. Garraffo and J. Carpenter for their help with some of the figures, and L. Smith for her careful editing of the manuscript. Finally, the authors would like to thank one of the reviewers for constructive comments and suggestions.

#### REFERENCES

- Arakawa, A., 1966: Computational design for long-term numerical integration of the equations of fluid motion: Two dimensional incompressible flow. Part I. *J. Comput. Phys.*, **1**, 119–143.
- Arhan, M., 1987: On the large scale dynamics of the Mediterranean outflow. *Deep-Sea Res.*, **34**, 1187–1208.
- Baringer, M. O., and J. F. Price, 1997a: Mixing and spreading of the Mediterranean outflow. *J. Phys. Oceanogr.*, **27**, 1654–1677.
- , and —, 1997b: Momentum and energy balance of the Mediterranean outflow. *J. Phys. Oceanogr.*, **27**, 1678–1692.
- Barnier, B., B. L. Hua, and C. Le Provost, 1991: On the catalytic role of high baroclinic modes in eddy-driven large-scale circulation. *J. Phys. Oceanogr.*, **21**, 976–997.
- Beckmann, A., C. W. Böning, B. Brüggemann, and D. Stammer, 1994: On the generation and role of eddy variability in the central North Atlantic Ocean. *J. Geophys. Res.*, **99**, 20 381–20 391.
- Bleck, R., and E. P. Chassignet, 1994: Simulating the oceanic circulation with isopycnal coordinate models. *The Oceans: Physiochemical Dynamics and Resources*, The Pennsylvania Academy of Science, 17–39.
- Boudra, D. B., and E. P. Chassignet, 1988: Dynamics of Agulhas Retroreflection and ring formation in a numerical model. Part I. The vorticity balance. *J. Phys. Oceanogr.*, **18**, 304–319.
- Bryden, H. L., and T. H. Kinder, 1991: Steady two-layer exchange through the Strait of Gibraltar. *Deep-Sea Res.*, **38** (Suppl.), S445–S463.
- , E. C. Brady, and R. D. Pillsbury, 1989: Flow through the Strait of Gibraltar. *Seminario Sobre La Oceanografía Física Del Estrecho De Gibraltar, Madrid*, 166–194.
- Chapman, D. C., 1985: Numerical treatment of cross-shelf open

- boundaries in a barotropic coastal ocean model. *J. Phys. Oceanogr.*, **15**, 1060–1075.
- Chassignet, E. P., and P. R. Gent, 1991: The influence of boundary conditions on midlatitude jet separation in ocean numerical models. *J. Phys. Oceanogr.*, **21**, 1290–1299.
- Cromwell, D., P. F. Challenor, and A. L. New, 1996: Persistent westward flow in the Azores Current as seen from altimetry and hydrography. *J. Geophys. Res.*, **101**, 11 923–11 933.
- Dengg, J., 1993: The problem of Gulf Stream separation: A barotropic approach. *J. Phys. Oceanogr.*, **23**, 2182–2200.
- Dietrich, G., K. Kalle, W. Kraus, and G. Siedler, 1975: *General Oceanography*. John Wiley, 626 pp.
- Gazdag, J., 1976: Time-differencing schemes and transform methods. *J. Comput. Phys.*, **20**, 196–207.
- Gould, W. J., 1985: Physical oceanography of the Azores Front. *Progress in Oceanography*, Vol. 14, Pergamon, 167–190.
- Haidvogel, D. B., J. C. McWilliams, and P. R. Gent, 1992: Boundary current separation in a quasigeostrophic, eddy-resolving ocean circulation model. *J. Phys. Oceanogr.*, **22**, 882–902.
- Hogg, N. G., and W. E. Johns, 1995: Western boundary currents. *Rev. Geophys.*, **33** (Suppl.), 1311–1334.
- Holland, W. R., and W. J. Schmitz, 1985: Zonal penetration scale of model midlatitude jets. *J. Phys. Oceanogr.*, **15**, 1859–1875.
- Howe, M. R., 1984: Current and hydrographical measurements in the Mediterranean Undercurrent near Cape St. Vincent. *Oceanol. Acta*, **7**, 163–168.
- Iorga, M. C., and M. S. Lozier, 1999a: Signatures of the Mediterranean outflow from a North Atlantic climatology. I: Salinity and density fields. *J. Geophys. Res.*, **104**, 25 985–26 009.
- , and —, 1999b: Signatures of the Mediterranean outflow from a North Atlantic climatology. 2: Diagnostic velocity fields. *J. Geophys. Res.*, **104**, 26 011–26 029.
- Jia, Y., 2000: On the formation of an Azores Current due to Mediterranean overflow in a modelling study of the North Atlantic. *J. Phys. Oceanogr.*, **30**, 2342–2358.
- Käse, R. H., and G. Siedler, 1982: Meandering of the subtropical front south-east of the Azores. *Nature*, **300**, 245–246.
- , and W. Krauss, 1996: The Gulf Stream, the North Atlantic Current, and the origin of the Azores Current. *The Warmwater Sphere of the North Atlantic Ocean*, W. Krauss, Ed., Gebrüder Borntraeger, 291–331.
- , W. Zenk, T. B. Sanford, and W. Hiller, 1985: Currents, fronts and eddy fluxes in the Canary Basin. *Progress in Oceanography*, Vol. 14, Pergamon, 231–257.
- Kinder, T. H., and H. L. Bryden, 1987: The 1985–1986 Gibraltar Experiment: Data collection and preliminary results. *Eos, Trans. Amer. Geophys. Union*, **68**, 786–787, 793–795.
- Klein, B., and G. Siedler, 1989: On the origin of the Azores Current. *J. Geophys. Res.*, **94**, 6159–6168.
- Le Traon, P.-Y., and P. De Mey, 1994: The eddy field associated with the Azores Front east of the Mid-Atlantic Ridge as observed by the Geosat altimeter. *J. Geophys. Res.*, **99**, 9907–9923.
- Levitus, S., 1982: *Climatological Atlas of the World Ocean*. NOAA Prof. Paper No. 13, U.S. Govt Printing Office 173 pp. and 17 microfiche.
- Mauritzen, C., Y. Morel, and J. Paillet, 2000: On the influence of Mediterranean Water on the Central Waters of the North Atlantic Ocean. *Deep-Sea Res.*, in press.
- Moore, D. W., 1963: Rossby waves in ocean circulation. *Deep-Sea Res.*, **10**, 735–747.
- Olbers, D. J., M. Wenzel, and J. Willebrand, 1985: The inference of North Atlantic circulation patterns from climatological hydrographic data. *Rev. Geophys.*, **23**, 313–356.
- Onken, R., 1993: The Azores Countercurrent. *J. Phys. Oceanogr.*, **23**, 1638–1646.
- Orlanski, I., 1976: A simple boundary condition for unbounded hyperbolic flows. *J. Comput. Phys.*, **41**, 115–135.
- Özgökmen, T. M., E. P. Chassignet, and A. M. Paiva, 1997: Impact of wind forcing, bottom topography, and inertia on midlatitude jet separation in a quasigeostrophic model. *J. Phys. Oceanogr.*, **27**, 2460–2476.
- Paiva, A. M., E. P. Chassignet, and A. J. Mariano, 2000: Numerical simulations of the North Atlantic subtropical gyre: Sensitivity to boundary conditions. *Dyn. Atmos. Oceans*, **32**, 209–237.
- Pedlosky, J., 1983: Eastern boundary ventilation and the structure of the thermocline. *J. Phys. Oceanogr.*, **13**, 2460–2476.
- , 1996: *Ocean Circulation Theory*. Springer, 405–408.
- Rhines, P. B., and W. Young, 1982: A theory of wind-driven circulation. Part I: Mid-ocean gyres. *J. Mar. Res.*, **40**, 559–596.
- Rios, A. F., F. F. Perez, and F. Fraga, 1992: Water masses in the upper and middle North Atlantic Ocean east of the Azores. *Deep-Sea Res.*, **39**, 645–658.
- Schmitz, W. J., Jr., and M. S. McCartney, 1993: On the North Atlantic circulation. *Rev. Geophys.*, **31**, 29–49.
- , J. D. Thompson, and J. R. Luyten, 1992: The Sverdrup circulation for the Atlantic along 24°N. *J. Geophys. Res.*, **97**, 7251–7256.
- Spall, M., 1990: Circulation in the Canary Basin: A model/data analysis. *J. Geophys. Res.*, **95**, 9611–9628.
- , 2000: Large-scale circulations forced by mixing near boundaries. *J. Mar. Res.*, in press.
- Stommel, H., 1982: Is the South Pacific helium plume dynamically active? *Earth Planet. Sci. Lett.*, **61**, 63–67.
- , and A. B. Arons, 1960a: On the abyssal circulation of the World Ocean. I: Stationary planetary flow patterns on a sphere. *Deep-Sea Res.*, **6**, 140–154.
- , and —, 1960b: On the abyssal circulation of the world ocean. II: An idealized model of the circulation pattern and amplitude in oceanic basins. *Deep-Sea Res.*, **6**, 271–233.
- , —, and A. J. Faller, 1958: Some examples of stationary flow patterns in bounded basins. *Tellus*, **10**, 179–187.
- Stramma, L., 1984: Geostrophic transport in the warm water sphere of the eastern subtropical North Atlantic. *J. Mar. Res.*, **42**, 537–558.
- , and T. J. Müller, 1989: Some observations of the Azores Current and the North Equatorial Current. *J. Geophys. Res.*, **94**, 3181–3186.
- Swallow, J. C., 1969: A deep eddy off Cape St. Vincent. *Deep Sea Res.*, **16** (Suppl.) 285–295.
- Townsend, T. L., H. E. Hurlburt, and P. J. Hogan, 2000: Modeled Sverdrup flow in the North Atlantic from eleven different wind stress climatologies. *Dyn. Atmos. Oceans*, **32**, 373–417.
- Verron, J., and E. Blayo, 1996: The no-slip condition and the separation of western boundary currents. *J. Phys. Oceanogr.*, **26**, 1938–1951.
- Weatherly, G. L., 1984: An estimate of bottom frictional dissipation by Gulf Stream fluctuations. *J. Mar. Res.*, **42**, 289–301.
- Woods, L. C., 1954: A note on the numerical solution of fourth order differential equations. *Aeronaut. Quart.*, **5**, 575–583.
- Worthington, L. V., 1976: On the North Atlantic circulation. *Oceanogr. Stud.*, **6**, 1–110.